CORRELATION OF PLASTIC DEFORMATION AND DYNAMIC RECRYSTALLIZATION IN MAGNESIUM ALLOY ZK60

A. GALIYEV[1, 2]†, R. KAIBYSHEV[1] and G. GOTTSTEIN[2]

[1]Institute for Metals Superplasticity Problems, Ufa 450001, Russia and [2]Institut für Metallkunde und Metallphysik, RWTH Aachen, Kopernikusstrasse 14, D-52056 Aachen, Germany

Abstract—The mechanisms of plastic deformation and dynamic recrystallization (DRX) in a Mg–5.8% Zn–0.65% Zr alloy were studied by compression tests at temperatures between 423 and 723 K and at strain rates ranging from 10^{-5} to 10^{-1} s^{-1}. It was shown that the mechanisms of DRX depended on the operating deformation mechanisms which changed with temperature. Low-temperature DRX (LTDRX below 473 K) was associated with the operation of twinning, basal slip and (**a**+**c**) dislocation glide. In the intermediate temperature range (473–523 K) continuous DRX (CDRX) was observed and associated with extensive cross-slip due to the Friedel–Escaig mechanism. At temperatures ranging from 573 to 723 K both bulging of original grain boundaries and subgrain growth were the operating DRX mechanisms and controlled by dislocation climb.

Keywords: Dislocations; Deformation mechanisms; Microstructure; Recrystallization & recovery

1. INTRODUCTION

Owing to growing interest in hot and warm thermomechanical working processes much research has been dedicated to the microstructural changes during dynamic recrystallization (DRX). Such studies have contributed essentially to improved industrial processing and a better understanding of the DRX process, at least on a phenomenological level. However, there is still a lack of understanding of the underlying physical processes that control DRX. In the following we present the results of a study on the DRX mechanisms in a magnesium alloy.

Like any recrystallization process, DRX proceeds by nucleation and nucleus growth. Nucleation frequently is the slowest process and, therefore, rate-controlling as for instance in magnesium [1]. Several DRX nucleation mechanisms have been proposed [2–10]. During hot deformation in many materials with low to medium stacking fault energy (SFE) [2–9], the formation of new grains occurs by conventional DRX—i.e., nucleation by bulging [4–8, 11], subgrain rotation [7, 9, 12] and twinning [8, 12]. Recently, a new mechanism of DRX was found to operate at low temperatures [10, 13]. These different mechanisms have been studied individually in the past, but little attention has been paid to the combined operation of various mechanisms of DRX in one material [8, 12]. Respective investigations indicated a correlation of the DRX mechanisms with deformation conditions. Since DRX occurs during deformation one ought to expect that the mechanisms of DRX are affected by the operating deformation processes. Surprisingly, little information about the deformation behavior and the concurrently activated mechanisms of DRX is available.

In a previous study [7] it was found that different mechanisms of DRX were operative in ZK60 magnesium alloy at different deformation temperatures. We utilized this information to examine the deformation behavior and the respective mechanisms of plastic deformation concurrently with the mechanisms of DRX, to elucidate the interdependence of deformation and DRX mechanisms in ZK60 magnesium alloy.

2. EXPERIMENTAL PROCEDURE

The ZK60 magnesium alloy used in the present study had a chemical composition of Mg–5.8% Zn–0.65% Zr (in wt%). The alloy (provided by Kamensk Uralsky Metallurgical Work, Russia) was fabricated by chill casting and solution treatment at 723 K for 6 h prior to deformation. The initial grain size was 85 μm. Two types of particle were contained in the equilibrium state of the magnesium alloy: globular ultrafine Zn_2Zr_3 and lamellar Mg_2Zn_3 phase (β phase).

Cylindrical specimens, 12 mm in length and 10 mm in diameter, were machined from the ingot. The specimens were deformed by uniaxial compression at constant displacement rate in an Instron mechanical testing machine. Tests were carried out at temperatures 423 K$\leq T \leq$723 K and strain rates 10^{-5} s$^{-1}\leq \dot{\varepsilon} \leq 10^{-1}$ s^{-1} using a graphite lubricant. All specimens were quenched in water *in situ* immediately after deformation.

The experimental procedures of microstructural and transmission electron microscopy (TEM) examinations are given in detail elsewhere [7, 14]. Specimens for surface examinations were first mechanically polished to create a flat section on a lateral surface, then chemically polished in a 30% solution of nitric acid in ethanol and finally electropolished in a 40% solution of orthophosphoric acid in ethanol at 4 V. After polishing these specimens were deformed to an additional strain of about 12% in air, and the surface features induced by plastic straining were studied by scanning electron microscopy (SEM) (JSM-840 instrument). Burgers vectors of dislocations were determined by the standard method of dislocation contrast analysis [15] for the (0002) reflection using a JEM-2000EX transmission electron microscope at 200 kV.

3. RESULTS

3.1. Flow stress behavior

Flow curves for ZK60 magnesium alloy at different deformation temperatures are shown in Fig. 1. Typically, the flow stress increases to a maximum and then decreases to finally attain a steady state. Such flow behavior is characteristic for hot working accompanied by DRX [2, 3]. In more detail, specific differences in the shape of the curves are evident. At low temperatures (423 K) the flow curve exhibits high peak stress (σ_p) at a high peak strain (ε_p) and insignificant work softening after the peak. At higher temperatures (473 K, 523 K) σ_p and ε_p are still high but work softening is more pronounced. At high temperatures (573–623 K) steady state is attained after small σ_p and ε_p with little softening. At 723 K stationary deformation proceeds from small strains.

The temperature dependence of the peak stress σ_p and the steady-state flow stress σ_s is very similar (Fig. 2). In an Arrhenius plot both dependences do not follow a straight line, but the curves can be decomposed into three ranges of constant slope. Owing to the similar behavior of σ_p and σ_s we shall confine our consideration to σ_s in the following.

Commonly, steady-state flow is observed to follow a power-law behavior

$$\dot{\varepsilon}_s = A_1 \left(\frac{\sigma_s}{G}\right)^n \exp\left(-\frac{Q}{RT}\right). \qquad (1a)$$

In fact, straight lines are obtained in a double log plot [Fig. 3(a)] except for the lowest temperature (423 K) where the behavior is better represented by [Fig. 3(b)]

$$\dot{\varepsilon}_s = A_2 \exp\left(\beta\frac{\sigma_s}{G}\right) \exp\left(-\frac{Q}{RT}\right). \qquad (1b)$$

The exponent n rises from n = 4.5 at 723 K to n = 6 at 473 K and the power law breaks down at even lower temperatures. From the found strain-rate dependence of σ_s the apparent activation energy Q can be determined (Fig. 4). It rises from about 92 kJ mol^{-1} at low temperatures to 135 kJ mol^{-1} at high temperatures. An evaluation of the peak stress reveals similar activation parameters (Table 1).

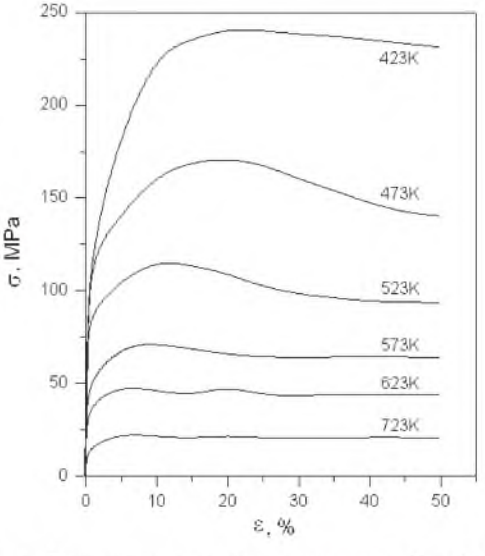

Fig. 1. Flow curves at various temperatures ($\dot{\varepsilon}$ = 2.8×10^{-3} s^{-1}).

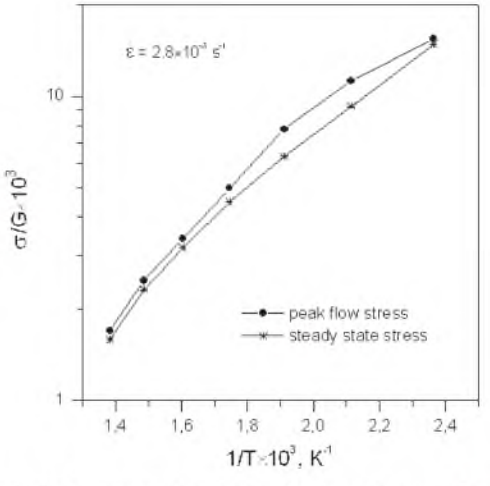

Fig. 2. The normalized stress as a function of reciprocal temperature.

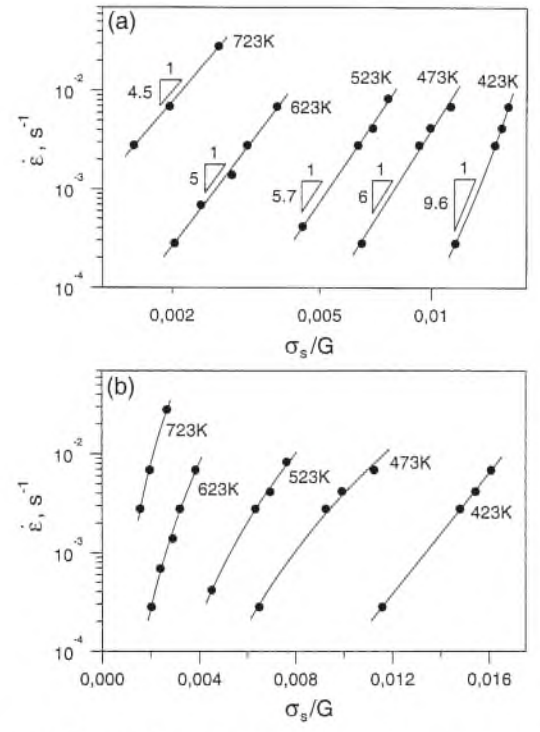

Fig. 3. The variation of the normalized steady-state stress with strain rate: (a) double log plot; (b) semi-logarithmic plot.

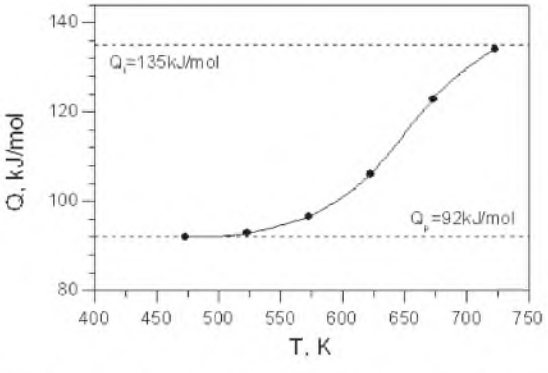

Fig. 4. Apparent activation energy as a function of temperature.

3.2. Slip systems

Surface observations on samples deformed at the low temperature of 423 K revealed twinning [7] and dislocation glide. Basal slip was dominant [Fig. 5(a)], but in addition short and thin slip lines inclined about 55° to the basal slip lines were observed [Fig. 5(b)]. Similar features were reported for specially oriented magnesium crystals deformed at low temperatures [16–18] and identified as non-basal slip lines. The non-basal slip traces coincided with $\{11\bar{2}2\}$ plane traces on the sample surface. TEM observations supported this conclusion [Fig. 6(a) and (b)]. The dislocation contrast was not extinguished for the (0002) reflection, hence the dislocation was of type of (**a**+**c**) with their edge component lying preferentially in the basal planes. Dislocation dipoles and loops also visible with the (0002) reflection could be attributed to double cross-slip of the screw kinks of (**a**+**c**) dislocations and splitting up of dipoles into a string of circular loops [16].

At T = 523 K basal and non-basal slip features were revealed within the original grains [Fig. 5(c)]. Short and wavy slip lines associated with cross-slip were found in deformed samples only near original grain boundaries [Fig. 5(d)] and were likely generated by cross-slip of **a** dislocations into non-basal planes [Fig. 6(c) and (d)]. Non-rectilinear dislocations lost their contrast with (0002) reflection and, therefore, were of **a** type lying both on basal and non-basal planes. The few dislocations not extinguished with the (0002) reflection might have been of (**a**+**c**) type.

At T = 623 K extensive multiple slip was observed within the original grains [Fig. 5(e) and (f)]. Surface observations in conjunction with TEM Burgers vector analysis allowed us to identify the observed slip lines as steps due to basal slip, **a** non-basal cross-slip and (**a**+**c**) non-basal slip [Fig. 6(e) and (f)]. The density of (**a**+**c**) dislocations decreased notably with rising temperature. Similar effects were reported for specially oriented magnesium crystals deformed in compression above 473 K [16].

3.3. Surface observations

Surface observations revealed features of nucleation of DRX during plastic deformation at intermediate and high temperatures. The nucleation of DRX at low temperatures was examined in detail in a previous work [7]. It was shown that twinning and progressive lattice rotations in areas of high dislocation density near twin boundaries resulted in the formation of fine grains with non-equilibrium grain boundaries. This grain formation mechanism is typical for plastic deformation of magnesium and magnesium alloys at lower temperatures [13, 19]. The

Table 1. Flow stress exponent and activation energy

	Temperature (K)			
	473	523	623	723
n_p/n_s	7.2/6	6.2/5.7	5/5	4.5/4.5
Q_p (kJ mol^{-1})	92	92	111	134
Q_s (kJ mol^{-1})	92	93	106	134

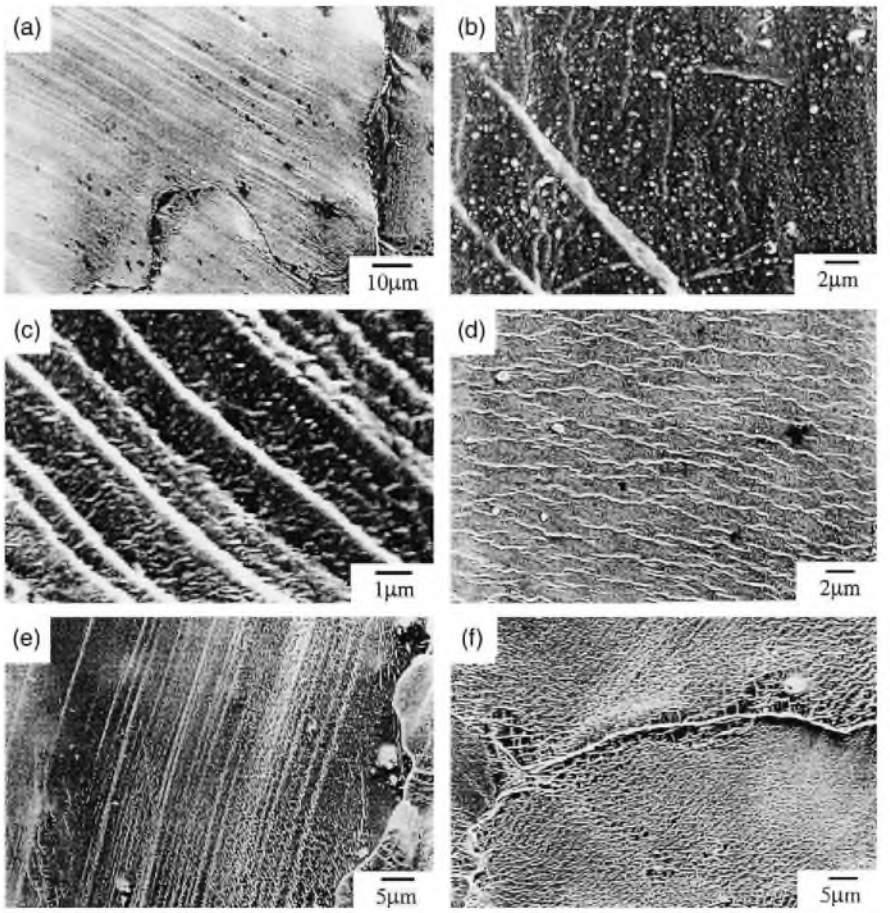

Fig. 5. SEM micrographs of deformation reliefs ($\varepsilon = 12\%$, $\dot{\varepsilon} = 2.8\times10^{-3}\ s^{-1}$). (a) $T = 423$ K, long straight lines of basal slip; (b) $T = 423$ K, short thin lines of $\{11\bar{2}2\}\langle\bar{1}\bar{1}23\rangle$ slip; (c) $T = 523$ K, lines of basal slip and non-basal slip within body of original grains; (d) $T = 523$ K, short wavy lines of **a** dislocation cross-slip; (e), (f) $T = 623$ K, extensive multiple slip.

nucleation of DRX at intermediate and high temperatures will be considered below.

At $T = 523$ K new grain boundaries were seen to be formed in non-basal slip areas near original boundaries where slip lines were identified as **a** dislocation cross-slip steps [Fig. 7(a)]. Since the cross-slip traces coincided with new grain boundaries, the dislocations probably accumulated in dislocation boundaries due to cross-slip through non-basal planes. Therefore, the formation of high-angle boundaries might be related with the operation of non-basal slip of **a** dislocations. Sub-boundaries can increase their misorientation by incorporation of crystal dislocations with increasing strain to high-angle boundaries [7]. As result, new grains formed a "necklace structure" of recrystallized grains along the original boundaries [Fig. 7(b)].

At temperatures ranging from 573 K to 723 K the formation of new grains was accompanied by the local migration of original grain boundaries [6, 7] in areas where extensive multiple slip bands had formed [Fig. 7(c) and (d)]. Grain boundary migration was accompanied by the formation of low-angle boundaries behind the swept volume which eventually cut off the expanding protrusion from the parent grain [Fig. 7(c)]. Therefore, new grain formation can be understood by the formation of a new boundary between ledges of a bulge. In general, new boundaries were formed in slip bands both near original grain boundaries and within original grains [Fig. 7(c) and (d)].

4. DISCUSSION

4.1. Deformation mechanisms

From dislocation structure evolution and flow stress behavior it is obvious that, in the temperature range investigated, different mechanisms of crystal plasticity operated and three different regimes have to be distinguished: (1) low temperature (below 473 K), (2) intermediate temperature (473–523 K), and (3) high temperature (above 523 K) range.

(1) At low temperatures basal slip and mechanical twinning were seen to accommodate the plastic strain. This is a classical combination of mechanisms for low-temperature deformation of alloys with hcp

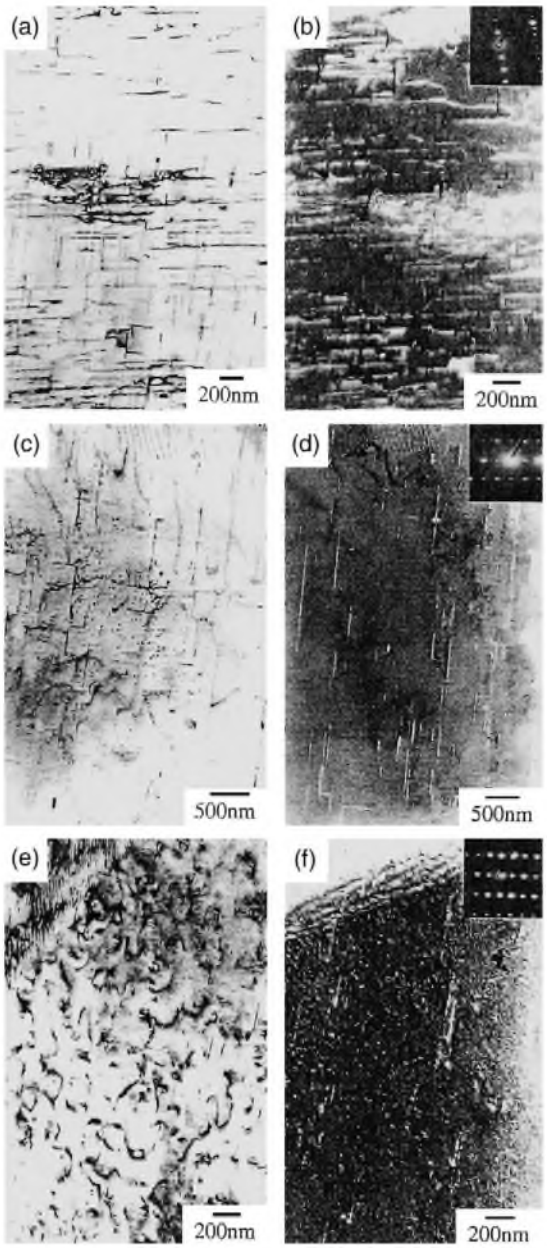

Fig. 6. Burgers vector analysis ($\varepsilon = 10\%$, $\dot{\varepsilon} = 2.8\times10^{-3}\ s^{-1}$). (a), (b) $T = 423$ K, (**a**+**c**) dislocations are visible in (0002) reflection; (c), (d) $T = 523$ K, non-rectilinear **a** dislocations are invisible for (0002) reflection, but (**a**+**c**) dislocations are visible for (0002) reflection; (e), (f) $T = 623$ K, non-rectilinear **a** dislocations are invisible for (0002) reflection. Note the reduction in density of (**a**+**c**) dislocations. (a), (c), (e) Bright-field images; (b), (d), (f) dark-field images.

lattice since the critical resolved shear stress on the basal plane is small and deformation twinning is readily activated. However, this combination can only insufficiently comply with the compatibility constraints at grain boundaries and the resulting high compatibility stresses may actually exceed locally the critical resolved shear stresses for non-basal slip, in particular on the $\{11\bar{2}2\}\langle\bar{1}\bar{1}23\rangle$ slip system [9, 18]. The hysteresis of local non-basal slip is supported by the substantial elongation to fracture and the occurrence of dynamic recovery, which requires the formation of three-dimensional (3D) dislocation structures. The low activation energy apparently reflects the need for non-conservative dislocation motion which requires diffusion, and only pipe diffusion can sufficiently contribute to mass transport at the low temperature. The power-law breakdown observed at 473 K occurred at a normalized strain rate of $\dot{\varepsilon}kT/D_L Gb \approx 10^{-4}\ s^{-1}$ and, therefore, at substantially larger values than predicted by the Sherby–Burke criterion ($10^{-8}\ s^{-1}$). This must be attributed to the considerably more complex dislocation geometry in hexagonal materials.

(2) The observed dislocation structures in the intermediate temperature regime can be associated with cross-slip-assisted dislocation glide as apparent from the dislocation geometry observed. Also the activation energy Q is observed to be dependent on temperature in this regime differently from the high-temperature regime. Friedel and Escaig [20, 21] proposed a mechanism for cross-slip of a basal **a** dislocation in hexagonal crystal structures. From a detailed calculation Couret *et al.* [22] obtained the activation energy

$$Q_{FE} = 2U_h + 2U_h' + 2l\Delta E + E_{el}(l, h, S) - \tau bh(S + l), \quad (2)$$

where $2U_h$ and $2U_h'$ are the energies of two half-constrictions in the basal plane and cross-slipped segment [22], respectively, ΔE is the difference between the energy per unit length of an extended segment in the basal plane and a constricted segment in the cross-slip plane [21], $E_{el}(l, h, S)$ is the elastic energy of the jog pair with jog height h, jog length l and the length of the re-extended segment S [22], τ is the resolved shear stress in the cross-slip plane and the last term in equation (2) represents the external work done in forming the jog pair.

Using the calculation from Refs. [21, 22] for the corresponding values in equation (2), Q_{FE} was calculated for the current experiments on ZK60 magnesium alloy (Fig. 8). The splitting width d/b is unknown, but for $d/b = 5$, the activation energy in the high-stress (intermediate-temperature) regime gives good agreement with the experimental results.

(3) At lower stresses (higher temperatures) the activation energy increases continuously up to $Q = 134\ kJ\ mol^{-1}$, which is close to that for magnesium volume self-diffusion. Apparently, the deformation behavior in the high-temperature range is diffusion-controlled and in context with the stress exponent $n \approx 5$ likely accompanied by dislocation climb. Raj and Langdon [23] have considered the transition from low-temperature climb to high-temperature climb. If the low-temperature process is now assumed to be Friedel–Escaig cross-slip, the effective activation energy for two competing processes can be written as

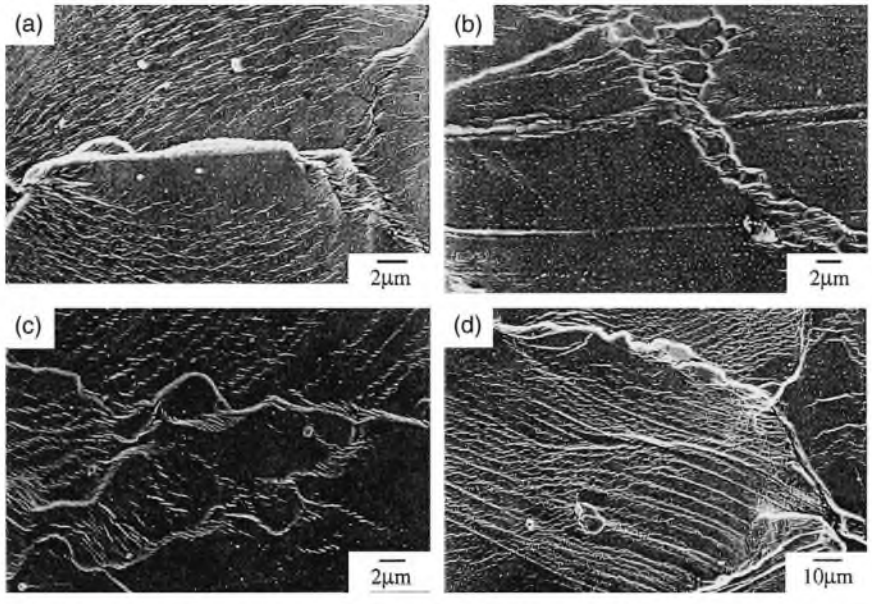

Fig. 7. Surface observations ($\dot{\varepsilon} = 2.8\times10^{-3}\ s^{-1}$), (a) $T = 523$ K, $\varepsilon = 12\%$, a cross-slip dislocations array in new grain boundaries; (b) $T = 523$ K, $\varepsilon = 25\%$, new grain formation near original boundary; (c) $T = 623$ K, $\varepsilon = 12\%$, slip band cuts off a protrusion; (d) $T = 723$ K, $\varepsilon = 12\%$, grain boundary migration toward slip band direction. Note in (c) and (d) formation of grain boundaries in slip bands.

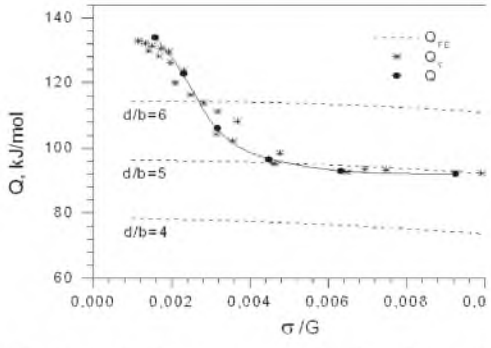

Fig. 8. True activation energy as a function of normalized stress.

$$Q_c = (Q_l\dot{\varepsilon}_{HT} + Q_p\dot{\varepsilon}_{FE})/(\dot{\varepsilon}_{HT} + \dot{\varepsilon}_{FE}), \qquad (3)$$

where $\dot{\varepsilon}_{HT}$ and $\dot{\varepsilon}_{FE}$ represent the strain rates for high-temperature climb and Friedel–Escaig cross-slip, respectively. These strain rates are given by

$$\dot{\varepsilon}_{HT} = A_1(D_lGb/kT)(\sigma/G)^5 \qquad (4)$$

and

$$\dot{\varepsilon}_{FE} = \beta A_1\exp(-Q_{FE}/RT)(\sigma/G)^7, \qquad (5)$$

where D_l is the appropriate diffusion coefficient, and A_1 and β are constants. Using equations (3) to (5), $\beta\approx10^{-3}$ and the value of Q_l for the diffusion coefficient ($D = D_0\exp(-Q/RT)$, with $D_0 = 10^{-4}\ m^2\ s^{-1}$ for lattice diffusion [24]), the magnitude of Q_c was calculated. The dependency of activation energy on stress (Fig. 8) is in good agreement with the experimental observations. The complicated temperature dependency of the activation energy for steady-state deformation can, therefore, be associated with the operation of different deformation mechanisms at different temperatures.

4.2. *Onset of dynamic recrystallization*

The peak stress and the steady-state flow stress were found to behave in a similar way (Fig. 2, Table 1). Since the steady-state flow stress could be associated with the deformation mechanisms predominant in the respective temperature regimes, obviously the peak stress also has to be related to the activated deformation mechanisms. The stress peak is caused by a superposition of hardening by dislocation storage and softening by dynamic recrystallization (DRX). Therefore, it is a measure for the onset of DRX, although the true onset of DRX has to occur somewhat before the peak, as will be addressed below. In fact, the development of the dynamically recrystallized microstructure reveals again three distinct temperature regimes, in analogy to the stationary flow behavior. For instance, the recrystallized grain size varies differently with the stress peak in three temperature ranges as reflected by the dependence of recrystallized grain size on the Zener–Hollomon parameter, $Z = \dot{\varepsilon}\exp(Q/RT)$ [Fig. 9(a) and (b)].

The stress peak is not identical with the onset of DRX, rather reduction of DRX has to occur before ε_p is reached. From principles of irreversible thermodynamics, Poliak and Jonas [25] proposed to associ-

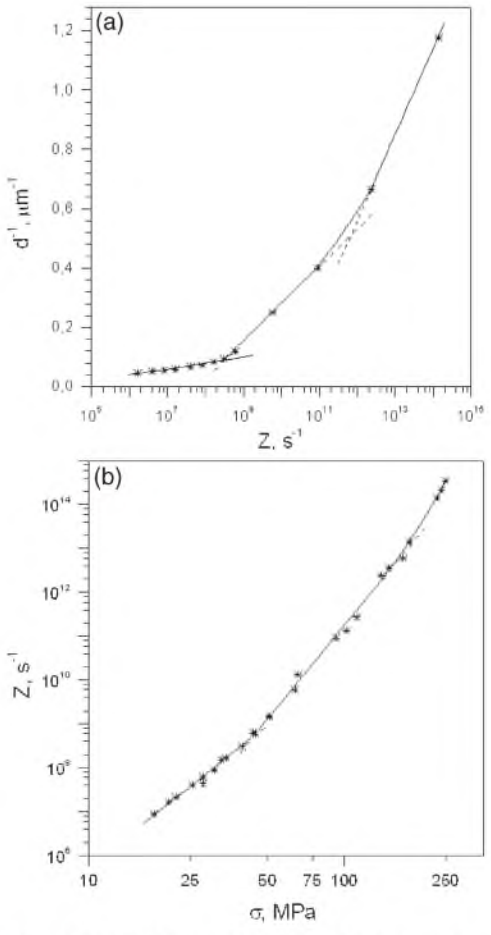

Fig. 9. Relationships between (a) inverse of recrystallized grain size and Zener–Hollomon parameter and (b) Zener–Hollomon parameter and flow stress.

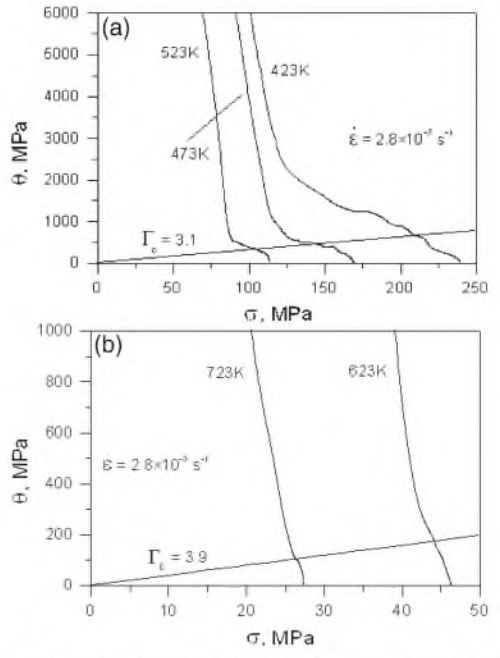

Fig. 10. The flow stress dependence of the strain-hardening rate at different temperatures: (a) from 423 K to 523 K; (b) 623 K and 723 K.

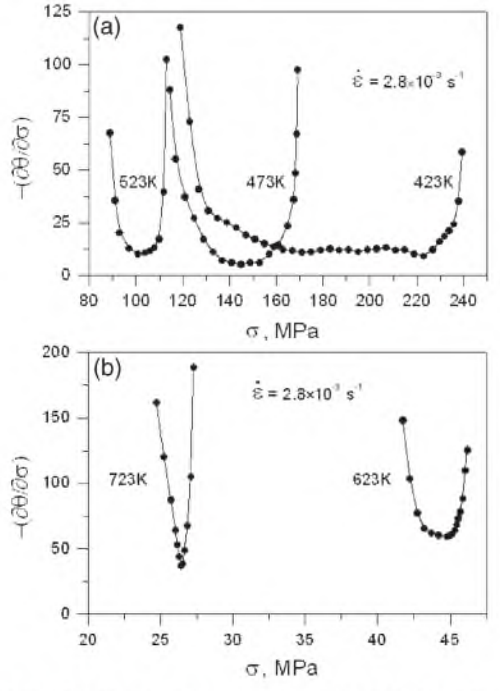

Fig. 11. The flow stress dependence of $-(\partial\theta/\partial\sigma)$ at different temperatures: (a) from 423 K to 523 K; (b) 623 K and 723 K.

ate the onset of DRX with the point on the hardening curve where, at maximum energy storage, the dissipation rate is at a minimum. The corresponding location on the flow curve is defined by the point of inflection on the θ–σ plot ($\theta \equiv d\sigma/d\varepsilon$)—i.e., where $-d\theta/d\varepsilon$ has a minimum. The corresponding plots are given in Figs 10 and 11. For a constant strain-rate sensitivity this criterion can be also represented by a constant value of $\Gamma_c = d \ln \sigma/d\varepsilon$, which is indicated in Fig. 10. The value of Γ_c is different for the low- and intermediate- and the high-temperature regime and would be even smaller for 423 K. Obviously, the strain-rate sensitivity, and thus the deformation mechanisms, are different in the respective temperature regimes as found for the steady-state flow stress and the peak stress, and reflected by the temperature dependence of the stress exponent and activation energy. In essence, the changes in deformation mechanisms also cause a change of the nucleation mechanisms of DRX.

From the results of the current study, cross-slip and high-temperature climb were identified as controlling mechanisms for large-strain plastic flow in ZK60 magnesium alloy. On the other hand, dislocation cross-slip and climb are also important for the dynamic recovery processes during plastic deformation. Continuous DRX (CDRX) was seen to take place in the region where cross-slip controls the rate of plastic deformation. When high-temperature climb becomes rate-controlling conventional DRX occurs in

ZK60 magnesium alloy. Low-temperature DRX (LTDRX) takes place in the exponential creep-law regime, where basal slip, twinning and local Friedel–Escaig cross-slip are observed. We propose the following models to account for deformation behavior and mechanisms of DRX in the ZK60 magnesium alloy.

At the low temperature of 423 K [Fig. 12(a)] basal slip and deformation twinning operate to comply with strain compatibility at grain boundaries. Basal dislocations with **a** Burgers vector accumulate near twin boundaries [7]. The internal stresses due to the remaining large elastic distortion at the grain boundaries exceed locally the critical resolved shear stress for non-basal slip, which is much larger than for basal slip at low temperatures [9, 18]. The rearrangement of the dislocations results in the formation of high-angle boundaries containing a high density of grain boundary dislocations [Fig. 12(a)]. This process is currently under investigation; however, it is obvious that (**a**+**c**) dislocations are required for the formation of 3D recrystallization nuclei.

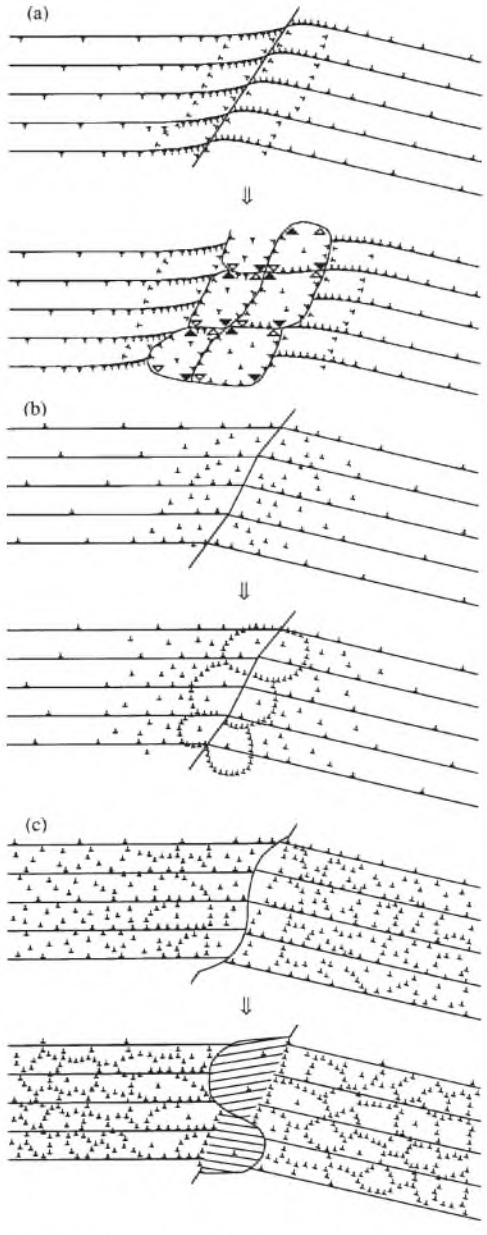

Fig. 12. Sketches of the nucleation process: (a) at T = 423 K ; (b) at T = 473–523 K; (c) at T = 573–723 K. [Note: for simplicity only **a** dislocations of one sign and no sub-boundary misorientation are shown in (b) and (c)].

At intermediate temperatures (473–523 K) the controlling mechanism of plastic deformation [Fig. 12(b)] is cross-slip of **a** dislocations on non-basal planes. This cross-slip is predominantly activated near original grain boundaries where the stresses are highly concentrated. The cross-slip of an **a** dislocation by the Friedel–Escaig mechanism leads to a transition from a primary screw orientation to an edge orientation [21, 26]. This edge dislocation lies in a non-basal plane, which is characterized by a high value of the stacking fault energy (SFE) [27, 28]. Therefore, this dislocation can readily climb. Dislocation rearrangements by cross-slip and climb generate a low-angle boundary network in the vicinity of original boundaries [7]. Continuous absorption of dislocations in the low-angle boundaries results in CDRX; i.e., in formation of new grains.

The ZK60 magnesium alloy is considered as a material with low SFE due to the fact that the SFE on the basal plane is low. At intermediate temperatures cross-slip results in the tranformation of most of dislocations located near original boundaries into non-basal dislocations on slip planes where the SFE is, at least, a factor of four larger [27, 28]. Therefore, CDRX—which normally occurs in materials with high values of SFE—also takes place in this magnesium alloy. In essence, cross-slip of **a** dislocations by the Friedel–Escaig mechanism controls both plastic flow and nucleation of DRX.

At high temperatures (573–723 K) [Fig. 12(c)] the activation energy of plastic flow approaches the activation energy for volume self-diffusion; i.e., the controlling process is dislocation climb. Microscopic strain localization at slip lines causes formation of bulges of grain boundaries which leads to nucleation of DRX grains [6, 7] [Fig. 12(c)]. This mechanism predominates mainly at low strains [7]. At moderate and higher strains DRX occurs via nucleation in slip bands. In both cases fast dislocation climb leads to the formation of low-angle boundaries [7]. Moving dislocations are trapped by these sub-boundaries and gradually convert them into true high-angle boundaries. Dislocation climb is the controlling process both for plastic deformation and nucleation of DRX. This is also supported by the fact that the recrystallized grain size drops sharply when the nucleation of DRX ceases to be diffusion-controlled at lower temperatures [Fig. 9(a)].

The observed deformation mechanisms are mapped with regard to the deformation conditions in Fig. 13.

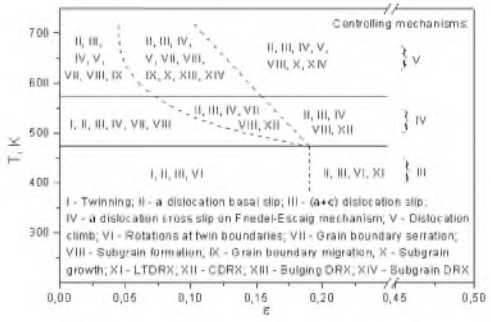

Fig. 13. Deformation and DRX mechanism map.

It is noted that the temperature can, of course, also be exchanged by the strain rate, $\ln \dot{\varepsilon}$.

5. CONCLUSIONS

1. The mechanisms of plastic deformation of magnesium alloy Mg–5.8% Zn–0.65% Zr were compared with the mechanisms of DRX at temperatures ranging from 423 to 723 K and strain rates between 10^{-5} and 10^{-1} s^{-1}.
2. It was found that the mechanisms of plastic deformation and DRX changed in similar temperature–strain rate regions as distinguished by deformation behavior and microstructure development.
3. At temperatures below 473 K, twinning, basal slip and (**a**+**c**) dislocation slip were found to operate. The operation of (**a**+**c**) slip promoted the formation of high-angle boundaries and LTDRX.
4. At intermediate temperatures of 473–523 K a power-law creep regime was observed with a stress exponent of about 7 and an activation energy of about 92 kJ mol^{-1}. The power-law breakdown occurred at a normalized strain rate about four orders of magnitude above the Sherby–Burke criterion. The activation energy for plastic deformation was associated with cross-slip of **a** dislocations according to the Friedel–Escaig mechanism. This resulted in CDRX.
5. At high temperatures of 573–723 K the value of the stress exponent was about 5, and the activation energy increased to a value close to the activation energy for magnesium self-diffusion. Dislocation climb controlled by self-diffusion is proposed to provide the conditions for the development of conventional DRX.
6. For the peak stress, steady-state flow stress and the stress to set off DRX, similar behavior was found with regard to their temperature behavior. In essence, there is substantial evidence that the mechanisms of nucleation of DRX and the mechanisms controlling steady-state deformation are closely related.

Acknowledgements—One of the authors (A.G.) wishes to express his gratitude to the Alexander von Humboldt Foundation for the award of a research fellowship.

REFERENCES

1. Sivakesavam, O., Rao, I. S. and Prasad, Y. V. R. K., *Mater. Sci. Technol.*, 1993, **9**, 805.
2. Sakai, T. and Jonas, J. J., *Acta metall.*, 1984, **32**, 189.
3. Humphreys, F. J. and Hatherley, M., in *Recrystallization and Related Annealing Phenomena*. Pergamon Press, Oxford, 1996, p. 363.
4. Miura, H., Aoyama, H. and Sakai, T., *J. Japan Inst. Met.*, 1994, **58**, 269.
5. Belyakov, A., Miura, H. and Sakai, T., *Mater. Sci. Eng.*, 1998, **A255**, 139.
6. Kaibyshev, R. O. and Sitdikov, O. S., *Phys. Met. Metallogr.*, 1994, **78**, 420.
7. Galiev, A. and Kaibyshev, R., to be published.
8. Kaibyshev, R. O. and Sitdikov, O. S., *Phys. Met. Metallogr.*, 1992, **73**, 635.
9. Ion, S. E., Humphreys, F. J. and White, S. H., *Acta metall.*, 1982, **30**, 1909.
10. Belyakov, A. and Kaibyshev, R., *Nanostruct. Mater.*, 1995, **6**, 893.
11. Gottstein, G., Chang, L. and Yung, H. F., *Mater. Sci. Technol.*, 1991, **7**, 158.
12. Gottstein, G. and Kocks, U. F., *Acta metall.*, 1983, **31**, 175.
13. Galiev, A., Kaibyshev, R. and Sitdikov, O., *Nanostruct. Mater.*, 1995, **6**, 621.
14. Kaibyshev, R. O., Galiev, A. M. and Sokolov, B. K., *Phys. Met. Metallogr.*, 1994, **78**, 209.
15. Bushnev, L. S., Kolobov, Y. C. and Myshlyaev, M. M., *Principles of Electron Microscopy*. Tomsk University, Tomsk, 1989, p. 218.
16. Obara, T., Yoshinga, H. and Morozumi, S., *Acta metall.*, 1973, **21**, 845.
17. Yoo, M. H., *Metall. Trans.*, 1981, **12**, 409.
18. Stohr, J. and Poirier, J., *Phil. Mag.*, 1972, **25**, 1313.
19. Valiev, R. Z., Krasilnikov, N. A. and Tsenev, N. K., *Mater. Sci. Eng.*, 1991, **A137**, 35.
20. Friedel, J., in *Internal Stresses and Fatigue in Metals*, Elsevier, Amsterdam, 1959, p. 220.
21. Escaig, B., *Phys. stat. sol.*, 1968, **28**, 463.
22. Couret, A., Caillard, D., Puschl, W. and Schoeck, G., *Phil. Mag. A.*, 1991, **63**, 1045.
23. Raj, S. V. and Langdon, T. G., *Acta metall.*, 1989, **37**, 843.
24. Frost, H. J. and Ashby, M. F., *Deformation-Mechanism Maps*. Metallurgiya, Chelyabinsk, 1989, p. 328.
25. Poliak, E. I. and Jonas, J. J., *Acta mater.*, 1996, **44**, 127.
26. Couret, A. and Caillard, D., *Acta metall.*, 1985, **33**, 1447.
27. Legrand, B., *Phil. Mag. A*, 1984, **49**, 171.
28. Puschl, W., Schoeck, G. and Kirchner, H. O. K., *Phil. Mag. A.*, 1987, **56**, 533.